

KK MC 4.22: CEEX EW Corrections for $f\bar{f} \rightarrow f'\bar{f}'$ at LHC and Muon Colliders

S. Jadach,^{1,2} B.F.L. Ward,¹ and Z. Was²

¹*Baylor University, Waco, TX, USA*

²*Institute of Nuclear Physics, Polish Academy of Sciences,
ul. Radzikowskiego 152, 31-342 Cracow, Poland*

We present the upgrade of the coherent exclusive (CEEX) exponentiation realization of the Yennie-Frautschi-Suura (YFS) theory used in our Monte Carlo ($\mathcal{K}\mathcal{K}$ MC) to the processes $f\bar{f} \rightarrow f'\bar{f}'$, $f = \mu, \tau, q, \nu_\ell$, $f' = e, \mu, \tau, q, \nu_\ell$, $q = u, d, s, c, b, t$, $\ell = e, \mu, \tau$ with $f \neq f'$, with an eye toward the precision physics of the LHC and possible high energy muon colliders. We give a brief summary of the CEEX theory in comparison to the older (EEX) exclusive exponentiation theory and illustrate theoretical results relevant to the LHC and possible muon collider physics programs.

PACS numbers: 12.38.-t, 12.38.Bx, 12.38.Cy

Keywords: QED, Electroweak, Monte Carlo

CONTENTS

I. Introduction	1
II. Review of Standard Model calculations for e^+e^- annihilation with YFS exponentiation	2
III. Extension of $\mathcal{K}\mathcal{K}$ MC to the processes $f\bar{f} \rightarrow f'\bar{f}'$, $f = \mu, q, \nu_\ell$, $f' = \ell, \nu_\ell, q$, $q = u, d, s, c, b$, $\ell = e, \mu, \tau$, $f \neq f'$,	4
IV. Conclusions	9
A. Sample Monte Carlo events	10
References	12

I. INTRODUCTION

Given that the era of precision QCD at the LHC is upon us, by which we mean theoretical precision tags at or below 1% in QCD corrections to LHC physical processes, computation of higher order EW corrections are also required: in the single Z production process at the LHC for example, a u quark anti-u quark annihilation hard process at the Z pole has a radiation probability strength factor of $\frac{4}{9} \frac{2\alpha}{\pi} (\ln(M_Z^2/m_u^2) - 1) \cong 0.038$ if we use the value $m_u \cong 5.0$ MeV, the current quark mass value – we return to the best choice for the quark masses below. Evidently, we have to take these EW effects into account at the per mille level if we do not wish that they spoil the sub-1% precision QCD we seek in LHC precision QCD studies [1]. Indeed, when the cut on the respective energy of the emitted photons is at ν_{min} in units of the reduced cms effective beam energy, the 0.038 strength factor above is enhanced to $0.038 \ln(1/\nu_{min})$ and can easily become $O(1)$. This means we have to use resummation, realized by MC event generator methods, of the type we have pioneered in Refs. [2] to make

contact with observation based on arbitrary cuts in any precise way. We call the reader's attention here to the approaches of Refs. [3–7] to EW corrections to such heavy gauge boson production at the LHC. It is well-known from LEP studies [8] that using only the exact $O(\alpha)$ EW corrections is inadequate for per mille level accuracy on these corrections. Our studies below will show that this is still the case. This means that the approaches in Ref. [3, 5–7] must be extended to higher orders for precision LHC studies. We comment further below on the relation of our approach to that in Ref. [4] as well¹.

Presently, we recall that in the case of single Z/γ^* production in high energy e^+e^- annihilation our state of the art realization of such resummation is the CEEX YFS [11, 12] exponentiation we have realized by MC methods in the $\mathcal{K}\mathcal{K}$ MC² in Ref. [13]. We conclude that we therefore need to extend the incoming states that the $\mathcal{K}\mathcal{K}$ MC allows to include the incoming quarks and anti-quarks in the protons colliding at the LHC. Previous versions of $\mathcal{K}\mathcal{K}$ MC even though not adapted for the LHC were already found useful in estimations of theoretical systematic errors of other calculations [14, 15]. We denote the new version of $\mathcal{K}\mathcal{K}$ MC by version number 4.22, $\mathcal{K}\mathcal{K}$ MC 4.22. Our aims in the current discussion in its regard are to summarize briefly on the main features of YFS/CEEX exponentiation [12, 16] in the SM EW theory,

¹ We remind the reader that, as it is done in Ref. [4] for example, in the hadron collider environment, one can also use DGLAP-CS [9, 10] theory for the large QED corrections in the ISR, so that standard factorization methods are used to remove the big QED logs from the reduced hard cross sections and they occur in the solution of the QED evolution equations for the PDF's which can be solved from the quark mass m_q to the factorization scale $Q \simeq M_Z$ here because QED is an infrared free theory; in what follows, we argue that we improve on the treatment of such effects with resummation methods we discuss presently.

² The name $\mathcal{K}\mathcal{K}$ MC derives from the fact that the program was published in the last year of the second millenium, where we note that K is the first letter of the Greek word Kilo, and from the fact that two of us (S.J. and Z.W.) were located in Krakow, Poland and the other of us (B.F.L.W.) was located in Knoxville, TN, USA at the inception of the code.

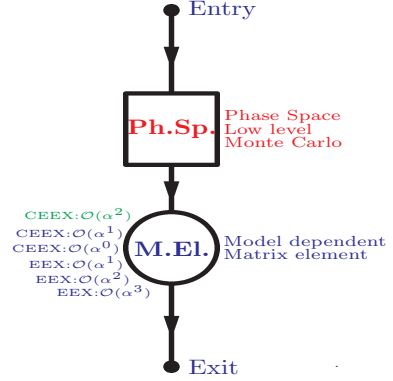
as this newer realization of the YFS theory is not a generally familiar one, to discuss the changes required to extend the incoming beam choices in the $\mathcal{K}\mathcal{K}$ MC from the original e^+e^- incoming state in Ref. [13] to the more inclusive choices $f\bar{f}$, $f = e, \mu, \tau, q, \nu_\ell$, $q = u, d, s, b$, $\ell = e, \mu, \tau$, and to present examples of theoretical results relevant for the LHC and possible muon collider [17] precision physics programs. For example, the muon collider physics program involves precision studies of the properties of the recently discovered BEH boson [18] candidate [19, 20] and treatment of the effects of higher order EW corrections will be essential to the success of the program, as we illustrate below.

In the next section, we review the older EEX exclusive realization and summarize the newer CEEX exclusive realization of the YFS [11] resummation in the SM EW theory; for, the YFS resummation is not generally familiar so that our review of the material in Refs. [2, 12, 16] will aid the unfamiliar reader to follow the current discussion. We do this in the context of e^+e^- annihilation physics programs for definiteness for historical reasons. In this way we illustrate the latter's advantages over the former, which is also very successful. We also stress the key common aspects of our MC implementations of the two approaches to exponentiation, such as the exact treatment of phase space in both cases, the strict realization of the factorization theorem, etc. We stress that both of the realizations of YFS exponentiation are available in the $\mathcal{K}\mathcal{K}$ MC 4.22 where both allow for the new incoming beams choices. This gives us important cross-check avenues required to establish the final precision tag of our results. In Sect. 3, we discuss and illustrate the extension of the choices of the incoming beams in the $\mathcal{K}\mathcal{K}$ MC realization of CEEX/EEX. We illustrate results which quantify the size of the EW higher order corrections in LHC and muon collider physics scenarios. Specific realizations of the results we present here in the context of a parton shower environment will appear elsewhere [21]. Sect. 4 contains our summary. Appendix 1 contains a sample output.

II. REVIEW OF STANDARD MODEL CALCULATIONS FOR e^+e^- ANNIHILATION WITH YFS EXPONENTIATION

There are many examples of successful applications [2] of our approach to the MC realization of the YFS theory of exponentiation for e^+e^- annihilation physics: (1), for $e^+e^- \rightarrow f\bar{f} + n\gamma$, $f = \tau, \mu, d, u, s, c$ there are YFS1 (1987-1989) $O(\alpha^1)_{exp}$ ISR, YFS2 \in KORALZ (1989-1990), $O(\alpha^1 + h.o.LL)_{exp}$ ISR, YFS3 \in KORALZ (1990-1998), $O(\alpha^1 + h.o.LL)_{exp}$ ISR+FSR, and $\mathcal{K}\mathcal{K}$ MC (98-02) $O(\alpha^2 + h.o.LL)_{exp}$ ISR+FSR+IFI with $d\sigma/\sigma = 0.2\%$; (2), for $e^+e^- \rightarrow e^+e^- + n\gamma$ for $\theta < 6^\circ$ there are BHLUMI 1.x, (1987-1990), $O(\alpha^1)_{exp}$ and BHLUMI 2.x,4.x, (1990-1996), $O(\alpha^1 + h.o.LL)_{exp}$ with $d\sigma/\sigma = 0.061\%$; (3), for $e^+e^- \rightarrow e^+e^- + n\gamma$ for $\theta > 6^\circ$ there is BHWIDE (1994-1998), $O(\alpha^1 + h.o.LL)_{exp}$ with $d\sigma/\sigma = 0.2(0.5)\%$ at the Z peak (just off the Z peak); (4), for $e^+e^- \rightarrow W^+W^- + n\gamma$, $W^\pm \rightarrow f\bar{f}$ there is KORALW (1994-2001); and, (5), for $e^+e^- \rightarrow W^+W^- + n\gamma$, $W^\pm \rightarrow f\bar{f}$ there is YFSWW3 (1995-2001), YFS exponentiation + Lead-

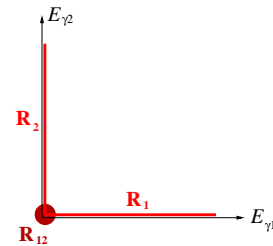
ing Pole Approximation with $d\sigma/\sigma = 0.4\%$ at LEP2 energies above the WW threshold. The typical MC realization we effect in Refs. [2] is in the form of the “matrix element \times exact phase space” principle, as we illustrate in the following diagram:



In practice it means the following:

- The universal exact Phase-space MC simulator is a separate module producing “raw events” (with importance sampling).
- The library of several types of SM/QED matrix elements which provides the “model weight” is another independent module (the $\mathcal{K}\mathcal{K}$ MC example is shown).
- Tau decays and hadronization come afterwards of course.

The main steps in YFS exponentiation are the reorganization of the perturbative complete $O(\alpha^\infty)$ series such that IR-finite β components are isolated (factorization theorem) and the truncation of the IR-finite β s to finite $O(\alpha^n)$ with the attendant calculation of them from Feynman diagrams recursively. We illustrate here the respective factorization for overlapping IR divergences for the 2γ case – $R_{12} \in R_1$ and $R_{12} \in R_2$ as they are shown in the following picture:



$$D_0(p_{f_1}, p_{f_2}, p_{f_3}, p_{f_4}) = \bar{\beta}_0(p_{f_1}, p_{f_2}, p_{f_3}, p_{f_4});$$

$$p_{f_1} + p_{f_2} = p_{f_3} + p_{f_4}$$

$$D_1(p_f; k_1) = \bar{\beta}_0(p_f) \tilde{S}(k_1) + \bar{\beta}_1(p_f; k_1);$$

$$p_{f_1} + p_{f_2} \neq p_{f_3} + p_{f_4}$$

$$D_2(k_1, k_2) = \bar{\beta}_0 \tilde{S}(k_1) \tilde{S}(k_2) + \bar{\beta}_1(k_1) \tilde{S}(k_2) + \bar{\beta}_1(k_2) \tilde{S}(k_1) + \bar{\beta}_2(k_1, k_2).$$

Note: $\bar{\beta}_0$ and $\bar{\beta}_1$ are used beyond their usual (Born and 1γ) respective phase spaces. A kind of smooth “extrapolation” or “projection” is always necessary. We see that a recursive order-by-order calculation of the IR-finite β s to a given fixed $O(\alpha^n)$ is possible: specifically,

$$\begin{aligned}\bar{\beta}_0(p_{f_1}, p_{f_2}, p_{f_3}, p_{f_4}) &= D_0(p_{f_1}, p_{f_2}, p_{f_3}, p_{f_4}), \\ \bar{\beta}_1(p_f; k_1) &= D_1(p_f; k_1) - \bar{\beta}_0(p_f) \tilde{S}(k_1), \\ \bar{\beta}_2(k_1, k_2) &= D_2(k_1, k_2) - \bar{\beta}_0 \tilde{S}(k_1) \tilde{S}(k_2) - \bar{\beta}_1(k_1) \tilde{S}(k_2) - \\ &\bar{\beta}_1(k_2) \tilde{S}(k_1), \dots, \text{allow such a truncation.}\end{aligned}$$

In the classic EEX/YFS schematically the β 's are truncated to $O(\alpha^1)$, in the ISR example. For $e^-(p_1, \lambda_1) + e^+(p_2, \lambda_2) \rightarrow f(q_1, \lambda'_1) + \bar{f}(q_2, \lambda'_2) + \gamma(k_1, \sigma_1) + \dots + \gamma(k_n, \sigma_n)$, we have

$$\sigma = \sum_{n=0}^{\infty} \int_{m_\gamma} d\Phi_{n+2} e^{Y(m_\gamma)} D_n(q_1, q_2, k_1, \dots, k_n) \quad (1)$$

with

$$\begin{aligned}D_0 &= \bar{\beta}_0, \quad D_1(k_1) = \bar{\beta}_0 \tilde{S}(k_1) + \bar{\beta}_1(k_1), \\ D_2(k_1, k_2) &= \bar{\beta}_0 \tilde{S}(k_1) \tilde{S}(k_2) + \bar{\beta}_1(k_1) \tilde{S}(k_2) + \bar{\beta}_1(k_2) \tilde{S}(k_1), \\ D_n(k_1, k_2, \dots, k_n) &= \bar{\beta}_0 \tilde{S}(k_1) \tilde{S}(k_2) \dots \tilde{S}(k_n) \\ &+ \bar{\beta}_1(k_1) \tilde{S}(k_2) \tilde{S}(k_3) \dots \tilde{S}(k_n) + \tilde{S}(k_1) \bar{\beta}_1(k_2) \tilde{S}(k_3) \dots \tilde{S}(k_n) \\ &+ \dots + \tilde{S}(k_1) \tilde{S}(k_2) \tilde{S}(k_3) \dots \bar{\beta}_1(k_n). \\ \sigma &= \sum_{n=0}^{\infty} \int_{m_\gamma} d\Phi_{n+2} \sum_{\lambda, \sigma_1, \dots, \sigma_n} |e^{\alpha B(m_\gamma)} \mathcal{M}_{n, \sigma_1, \dots, \sigma_n}^\lambda(k_1, \dots, k_n)|^2, \\ \mathcal{M}_{2, \sigma_1, \sigma_2}^\lambda(k_1, k_2) &= \hat{\beta}_0^\lambda \mathfrak{s}_{\sigma_1}(k_1) \mathfrak{s}_{\sigma_2}(k_2) + \hat{\beta}_{1, \sigma_1}^\lambda(k_1) \mathfrak{s}_{\sigma_2}(k_2) + \hat{\beta}_{1, \sigma_2}^\lambda(k_2) \mathfrak{s}_{\sigma_1}(k_1), \\ &+ \hat{\beta}_{1, \sigma_1}^\lambda(k_1) \mathfrak{s}_{\sigma_2}(k_2) \dots \mathfrak{s}_{\sigma_n}(k_n) + \mathfrak{s}_{\sigma_1}(k_1) \hat{\beta}_{1, \sigma_2}^\lambda(k_2) \dots \mathfrak{s}_{\sigma_n}(k_n) + \dots + \mathfrak{s}_{\sigma_1}(k_1) \mathfrak{s}_{\sigma_2}(k_2) \dots \mathfrak{s}_{\sigma_{n-1}}(k_{n-1}) \hat{\beta}_{1, \sigma_n}^\lambda(k_n),\end{aligned} \quad (2)$$

where λ is the collective index of fermion helicities. The $O(\alpha^1)$ IR-finite building blocks are:

$$\begin{aligned}\hat{\beta}_0^\lambda &= (e^{-\alpha B_4} \mathcal{M}_\lambda^{\text{Born+Virt.}})|_{O(\alpha^1)}, \\ \hat{\beta}_{1, \sigma}^\lambda(k) &= \mathcal{M}_{1, \sigma}^\lambda(k) - \hat{\beta}_0^\lambda \mathfrak{s}_\sigma(k)\end{aligned}$$

Everything above is expressed in terms of \mathcal{M} -amplitudes! Distributions are ≥ 0 by construction! In $\mathcal{K}\mathcal{K}\mathcal{MC}$ the above is done up to $O(\alpha^2)$ for ISR and FSR.

The full scale CEEX $O(\alpha^r)$, $r=1,2$, master formula for the polarized total cross section reads as follows:

$$\begin{aligned}\sigma^{(r)} &= \sum_{n=0}^{\infty} \frac{1}{n!} \int d\tau_n(p_a + p_b; p_c, p_d, k_1, \dots, k_n) \\ &\times e^{2\alpha \mathcal{R}B_4} \sum_{\sigma_i, \bar{\lambda}, \bar{\lambda}} \sum_{i, j, l, m=0}^3 \hat{\varepsilon}_a^i \hat{\varepsilon}_b^j \sigma_{\lambda_a \bar{\lambda}_a}^i \sigma_{\lambda_b \bar{\lambda}_b}^j \\ &\times \mathfrak{M}_n^{(r)}\left(\frac{pk_1}{\bar{\lambda} \sigma_1} \frac{k_2}{\sigma_2} \dots \frac{k_n}{\sigma_n}\right) \left[\mathfrak{M}_n^{(r)}\left(\frac{pk_1}{\bar{\lambda} \sigma_1} \frac{k_2}{\sigma_2} \dots \frac{k_n}{\sigma_n}\right)\right]^* \sigma_{\bar{\lambda}_c \lambda_c}^l \sigma_{\lambda_d \bar{\lambda}_d}^m \hat{h}_c^l \hat{h}_d^m.\end{aligned} \quad (5)$$

The real soft factors and the IR-finite building blocks are

$$\begin{aligned}\tilde{S}(k) &= \sum_{\sigma} |\mathfrak{s}_\sigma(k)|^2 = |\mathfrak{s}_+(k)|^2 + |\mathfrak{s}_-(k)|^2 \\ &= -\frac{\alpha}{4\pi^2} \left(\frac{q_1}{kq_1} - \frac{q_2}{kq_2} \right)^2 \\ \bar{\beta}_0 &= (e^{-2\alpha \mathcal{R}B_4} \sum_{\lambda} |\mathcal{M}_\lambda^{\text{Born+Virt.}}|^2)|_{O(\alpha^1)}, \\ \bar{\beta}_1(k) &= \sum_{\lambda \sigma} |\mathcal{M}_{\lambda \sigma}^{1-\text{PHOT}}|^2 - \sum_{\sigma} |\mathfrak{s}_\sigma(k)|^2 \sum_{\lambda} |\mathcal{M}_\lambda^{\text{Born}}|^2,\end{aligned} \quad (3)$$

with λ = fermion helicity, σ = photon helicity, and everything being in terms of $\sum_{spin} |\dots|^2$!

The newer CEEX replaces older the EEX, where both are derived from the YFS theory [11]: EEX, Exclusive EXponentiation, is very close to the original Yennie-Frautschi-Suura formulation, which is also now featured in the MC's Herwig++ [22] and Sherpa [23] for particle decays. We need to stress that CEEX, Coherent EXclusive exponentiation, is an extension of the YFS theory. Because of its coherence CEEX is friendly to quantum coherence among the Feynman diagrams, so that we have the complete $|\sum_{diag}^n \mathcal{M}_i|^2$ rather than the often incomplete $\sum_{i,j}^n \mathcal{M}_i \mathcal{M}_j^*$. It follows that we get readily the proper treatment of narrow resonances, $\gamma \oplus Z$ exchanges, $t \oplus s$ channels, $\text{ISR} \oplus \text{FSR}$, angular ordering, etc. KORALZ/YFS2, BHLUMI, BHWIDE, YFSWW, KoralW and KORALZ are examples of the EEX formulation in our MC event generator approach; $\mathcal{K}\mathcal{K}\mathcal{MC}$ is the only example of the CEEX formulation.

Using the example of ISR $O(\alpha^1)$ we illustrate CEEX schematically for the process $e^-(p_1, \lambda_1) + e^+(p_2, \lambda_2) \rightarrow f(q_1, \lambda'_1) + \bar{f}(q_2, \lambda'_2) + \gamma(k_1, \sigma_1) + \dots + \gamma(k_n, \sigma_n)$. We have

The respective CEEX amplitudes are

$$\begin{aligned}
\mathfrak{M}_n^{(1)}(p_{\lambda\sigma_1}^{k_1} \dots p_{\lambda\sigma_n}^{k_n}) &= \sum_{\emptyset \in \mathcal{P}} \prod_{i=1}^n \mathfrak{s}_{[i]}^{\{\emptyset_i\}} \left\{ \hat{\beta}_0^{(1)}(p; X_\emptyset) + \sum_{j=1}^n \frac{\hat{\beta}_1^{(1)}(\{ \emptyset_j \} (p_{\lambda\sigma_j}^{k_j}; X_\emptyset)}{\mathfrak{s}_{[j]}^{\{\emptyset_j\}}} \right\} \\
\mathfrak{M}_n^{(2)}(p_{\lambda\sigma_1}^{k_1} \dots p_{\lambda\sigma_n}^{k_n}) &= \sum_{\emptyset \in \mathcal{P}} \prod_{i=1}^n \mathfrak{s}_{[i]}^{\{\emptyset_i\}} \left\{ \hat{\beta}_0^{(2)}(p; X_\emptyset) + \sum_{j=1}^n \frac{\hat{\beta}_1^{(2)}(\{ \emptyset_j \} (p_{\lambda\sigma_j}^{k_j}; X_\emptyset)}{\mathfrak{s}_{[j]}^{\{\emptyset_j\}}} + \sum_{1 \leq j < l \leq n} \frac{\hat{\beta}_2^{(2)}(\{ \emptyset_j, \emptyset_l \} (p_{\lambda\sigma_j}^{k_j} p_{\lambda\sigma_l}^{k_l}; X_\emptyset)}{\mathfrak{s}_{[j]}^{\{\emptyset_j\}} \mathfrak{s}_{[l]}^{\{\emptyset_l\}}} \right\}.
\end{aligned} \tag{6}$$

For the full details see ref. [12].

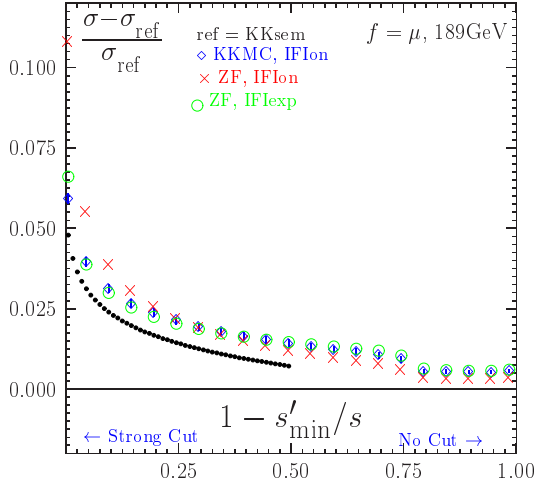


FIG. 1. Principal cross checks of \mathcal{KKMC} for $e^-e^+ \rightarrow \mu^-\mu^+ + n\gamma$ process at $\sqrt{s}=189\text{GeV}$.

The precision tags of the \mathcal{KKMC} are determined by comparisons with our own semi-analytical and independent MC results and by comparison with the semi-analytical results of the program ZFITTER [24]. In Fig. 1 we illustrate such comparisons, which lead to the \mathcal{KKMC} precision tag $d\sigma/\sigma = 0.2\%$ for example. The ISR of ZFITTER is based on the $O(\alpha^2)$ result of ref. [25], while \mathcal{KKMC} is totally independent! See Ref. [12, 26] for a more complete discussion. Thus, we know that \mathcal{KKMC} has the capability to deliver per mille precision on the large EW effects if it is extended to the appropriate incoming beams for the LHC and the muon collider. To this we now turn.

III. EXTENSION OF \mathcal{KKMC} TO THE PROCESSES

$$\begin{aligned}
f\bar{f} \rightarrow f'\bar{f}', f = \mu, q, \nu_\ell, f' = \ell, \nu_\ell, q, q = u, d, s, c, b, \\
\ell = e, \mu, \tau, f \neq f',
\end{aligned}$$

At the LHC and at a futuristic muon collider [17], the incoming beams involve for Z/γ^* production and decay the other light charged fundamental fermions in the SM: u, d, s, c, b for the LHC and the muon for a muon collider. Thus, we need to extend the matrix elements, residuals, and IR functions in (1,5) to the case where we substitute the e^-, e^+ EW charges by the new beam particles f, \bar{f} EW charges

and we substitute the mass m_e everywhere by m_f ³. We have done this with considerable cross checks against the same semi-analytical tools that we employed in Ref. [12] to establish the precision tag of version 4.13 of \mathcal{KKMC} . We want to stress that this was a highly non-trivial set of cross-checks: for example, we found that the MC procedure used in the crude MC cross section was unstable when the value of the radiation strength factor $\gamma_f = \frac{2Q_f^2\alpha}{\pi} \left(\ln(s/m_f^2) - 1 \right)$ becomes too small⁴. This instability was removed and the correct value of the MC crude cross section was verified by semi-analytical methods. We did therefore a series of cross checks/illustrations with the new version of \mathcal{KKMC} , version 4.22, which we now exhibit.

Turning first to the most important cross-check, we show in Tab. I and Figs. 2-4 that for the $e^+e^- \rightarrow \mu^+\mu^-$ process, our new version \mathcal{KKMC} 4.22 reproduces the results in the corresponding $\sqrt{s} = 189\text{GeV}$ cross checks done in Ref. [12] for the dependence of the CEEX calculated cross section and A_{FB} on the energy cut-off on $v = 1 - s'/s$ where $s' = M_{\mu\bar{\mu}}^2$ is the invariant mass of the $\mu\bar{\mu}$ -system. The reader can check that the two sets of results, those given here in Tab. I and Figs. 2-4 and those given in Table 5, Figs. 20,21, and 18 in Ref. [12] are in complete agreement within statistical fluctuations. This shows that our introduction of the new beams has not spoiled the precision of the \mathcal{KKMC} for the incoming e^+e^- state.

³ We advise the reader that especially in the QED radiation module KarLud for the ISR in \mathcal{KKMC} , see Ref. [13], some of the expressions had Q_e and m_e effectively hard-wired into them and these had to all be found and substituted properly.

⁴ In the case of the quarks, we will use here the current quark mass values $m_u \cong 5\text{MeV}$ and $m_d \cong 10\text{MeV}$ following Ref. [27] for our illustrations; we leave these values as user input in general.

v_{\max}	$\mathcal{K}\mathcal{K}\text{sem Ref.}$	$\mathcal{O}(\alpha^3)_{\text{EEX3}}$	$\mathcal{O}(\alpha^2)_{\text{CEEX intOFF}}$	$\mathcal{O}(\alpha^2)_{\text{CEEX}}$
$\sigma(v_{\max})$ [pb]				
0.01	1.6712 \pm 0.0000	1.6736 \pm 0.0018	1.6738 \pm 0.0018	1.7727 \pm 0.0021
0.10	2.5198 \pm 0.0000	2.5205 \pm 0.0020	2.5210 \pm 0.0020	2.6009 \pm 0.0024
0.30	3.0616 \pm 0.0000	3.0626 \pm 0.0022	3.0634 \pm 0.0022	3.1243 \pm 0.0026
0.50	3.3747 \pm 0.0000	3.3745 \pm 0.0022	3.3761 \pm 0.0022	3.4254 \pm 0.0026
0.70	3.7223 \pm 0.0000	3.7214 \pm 0.0022	3.7249 \pm 0.0022	3.7648 \pm 0.0027
0.90	7.1430 \pm 0.0000	7.1284 \pm 0.0022	7.1530 \pm 0.0022	7.1821 \pm 0.0026
0.99	7.6136 \pm 0.0000	7.5974 \pm 0.0021	7.6278 \pm 0.0021	7.6567 \pm 0.0026
$A_{\text{FB}}(v_{\max})$				
0.01	0.5654 \pm 0.0000	0.5661 \pm 0.0012	0.5661 \pm 0.0012	0.6121 \pm 0.0014
0.10	0.5664 \pm 0.0000	0.5667 \pm 0.0009	0.5667 \pm 0.0009	0.5931 \pm 0.0011
0.30	0.5692 \pm 0.0000	0.5694 \pm 0.0008	0.5693 \pm 0.0008	0.5864 \pm 0.0010
0.50	0.5744 \pm 0.0000	0.5744 \pm 0.0008	0.5743 \pm 0.0008	0.5870 \pm 0.0009
0.70	0.5863 \pm 0.0000	0.5858 \pm 0.0007	0.5857 \pm 0.0007	0.5953 \pm 0.0008
0.90	0.3105 \pm 0.0000	0.3107 \pm 0.0004	0.3100 \pm 0.0004	0.3176 \pm 0.0004
0.99	0.2851 \pm 0.0000	0.2856 \pm 0.0003	0.2848 \pm 0.0003	0.2918 \pm 0.0004

TABLE I. Energy cut-off study of total cross section σ and charge asymmetry A_{FB} for annihilation process $e^-e^+ \rightarrow \mu^-\mu^+$, at $\sqrt{s}=189\text{GeV}$. Energy cut: $v < v_{\max}$, $v = 1 - M_{f\bar{f}}^2/s$. Scattering angle for A_{FB} is θ^* (defined in Phys. Rev. **D41**, 1425 (1990)). No cut in θ^* . E-W corr. in $\mathcal{K}\mathcal{K}$ according to DIZET 6.x. In addition to CEEX matrix element, results are also shown for $\mathcal{O}(\alpha^3)_{\text{LL}}$ EEX3 matrix element without ISR \otimes FSR interf. $\mathcal{K}\mathcal{K}\text{sem}$ is semianalytical program, part of $\mathcal{K}\mathcal{K}\text{MC}$.

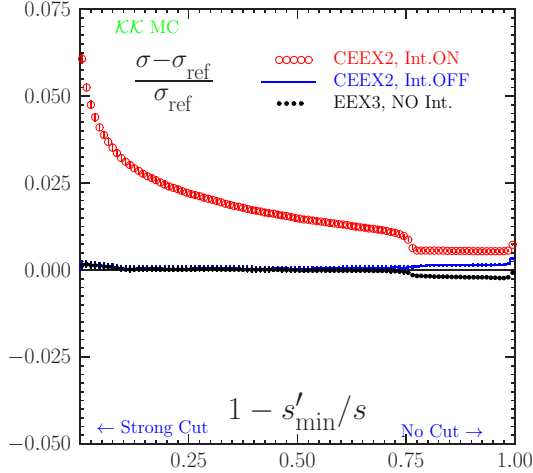


FIG. 2. Total cross section σ , energy cut-off study. The same results as in the Table I. Ref. σ_{ref} = semianalytical of $\mathcal{K}\mathcal{K}\text{sem}$.

We turn next to the new type of incoming beam scenario in Tab. II and Figs. 5-7 wherein we show the analogous results to those in Tab. I and Figs. 2-4 for the process $d\bar{d} \rightarrow \mu^-\mu^+$ at $\sqrt{s}=189\text{GeV}$ so that we can keep a good reference to the relative size of the EW corrections versus what one would have in the usual e^+e^- annihilation case. We see that for strong cuts, with $v_{\max} \sim .01$ and for the loose cut, with $v_{\max} \sim 0.99$, the effects are similar to those in the more familiar incoming e^+e^- annihilation case, as the sign of the EW charges are the same for the d and the e^- . The values are different so that size of the effects in Tab. II and Figs. 5-7 are correspondingly different. For example, in the strong cut, turning the initial-final state interference (IFI) off changes the CEEX cross section result for $v_{\max} = 0.01$ by -1.9% for the incom-

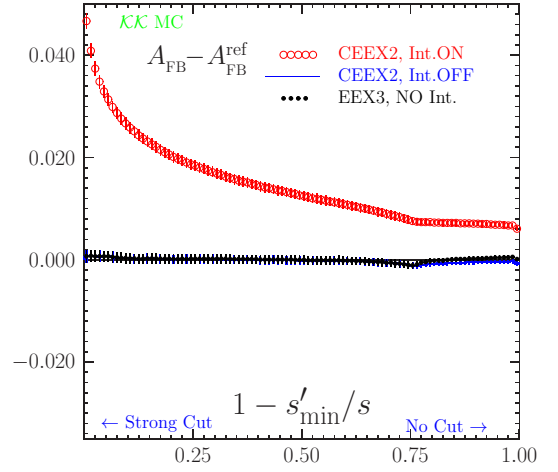


FIG. 3. Energy cut-off study of charge asymmetry A_{FB} for the process $e^+e^- \rightarrow \mu^+\mu^-$. The same results as in the Table I. Reference $A_{\text{FB}}^{\text{ref}}$ = semianalytical $\mathcal{K}\mathcal{K}\text{sem}$.

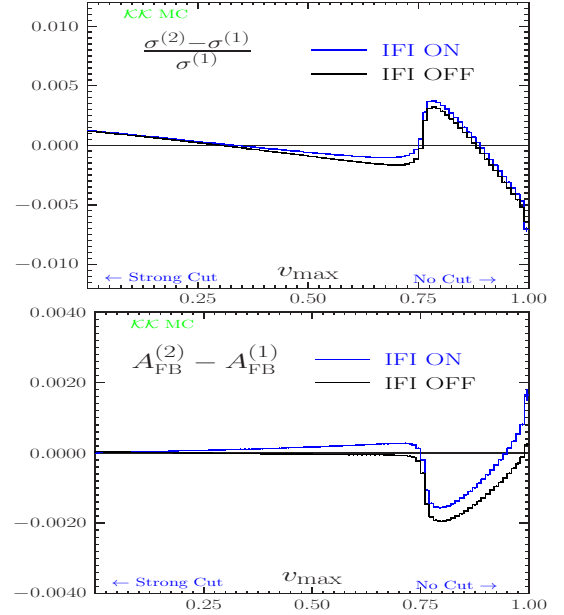


FIG. 4. Physical precision of CEEX ISR matrix element for $e^-e^+ \rightarrow \mu^-\mu^+$ at $\sqrt{s}=189\text{GeV}$. See table I for definition of cut-offs.

ing $d\bar{d}$ case compared to -5.9% for the incoming e^-e^+ case. The behavior of $A_{\text{FB}}(v_{\max})$ is similar between to the two incoming beam sets, where turning the IFI off reduces the value of A_{FB} at $v_{\max} = 0.01$ by 8.12% (2.55%) respectively for the incoming $e^-e^+(d\bar{d})$ case. In both cases, the loose cut such as $v_{\max} = 0.99$ tends to wash-out these effects. In Fig. 5 the data on the cross sections in the table in Tab. II are plotted in relation to the reference semi-analytical result denoted as $\mathcal{K}\mathcal{K}\text{sem}$ [12] as the ratio of their difference to the reference divided by the reference and in Fig. 6 the corresponding data on A_{FB} are plotted as their difference with the respective $\mathcal{K}\mathcal{K}\text{sem}$ results. When compared to the analogous results for the usual e^-e^+ case in Figs. 2 and 3 we see that structure at the

Z-radiative return position, $v_{\max} \cong 0.77$, is very much reduced in the $d\bar{d}$ case due to the smaller electric charge magnitude, just as the size of the IFI effects themselves are similarly reduced. In Fig. 7, we show the physical precision test which compares the size of the second and first order CEEX results for the cross section and the forward-backward asymmetry: for the $d\bar{d}$ case compared to the similar plots in Fig. 4 for the e^-e^+ case we see that for the strong cuts we have higher precision, we have smooth behavior through the Z-peak region, and that at the very loose cuts the two precision tags are similar, where we would estimate that similar value at 0.35% in the worst case that $v_{\max} \rightarrow 1$ on the cross section for example – here we use half the difference shown in the figure as the error estimate. For the more generic energy cut of 0.6% our physical precision estimate is 0.05%. This is the type of precision required for the precision LHC physics studies.

v_{\max}	$\mathcal{K}\mathcal{K}\text{sem Ref.}$	$\mathcal{O}(\alpha^3)_{\text{EEX3}}$	$\mathcal{O}(\alpha^2)_{\text{CEEX intOFF}}$	$\mathcal{O}(\alpha^2)_{\text{CEEX}}$
$\sigma(v_{\max})$ [pb]				
0.01	0.9145 \pm 0.0000	0.9150 \pm 0.0004	0.9150 \pm 0.0004	0.9323 \pm 0.0004
0.10	1.0805 \pm 0.0000	1.0807 \pm 0.0004	1.0808 \pm 0.0004	1.0920 \pm 0.0004
0.30	1.1612 \pm 0.0000	1.1615 \pm 0.0004	1.1616 \pm 0.0004	1.1691 \pm 0.0004
0.50	1.1974 \pm 0.0000	1.1977 \pm 0.0004	1.1981 \pm 0.0004	1.2036 \pm 0.0004
0.70	1.2310 \pm 0.0000	1.2312 \pm 0.0004	1.2317 \pm 0.0004	1.2357 \pm 0.0004
0.90	1.6104 \pm 0.0000	1.6128 \pm 0.0003	1.6114 \pm 0.0004	1.6148 \pm 0.0004
0.99	1.6218 \pm 0.0000	1.6254 \pm 0.0003	1.6244 \pm 0.0004	1.6277 \pm 0.0004
$A_{\text{FB}}(v_{\max})$				
0.01	0.5883 \pm 0.0000	0.5883 \pm 0.0005	0.5883 \pm 0.0005	0.6033 \pm 0.0005
0.10	0.5882 \pm 0.0000	0.5881 \pm 0.0004	0.5881 \pm 0.0004	0.5966 \pm 0.0004
0.30	0.5879 \pm 0.0000	0.5879 \pm 0.0004	0.5879 \pm 0.0004	0.5932 \pm 0.0004
0.50	0.5875 \pm 0.0000	0.5874 \pm 0.0004	0.5875 \pm 0.0004	0.5912 \pm 0.0004
0.70	0.5848 \pm 0.0000	0.5845 \pm 0.0004	0.5846 \pm 0.0004	0.5868 \pm 0.0004
0.90	0.4736 \pm 0.0000	0.4722 \pm 0.0003	0.4728 \pm 0.0003	0.4748 \pm 0.0003
0.99	0.4710 \pm 0.0000	0.4691 \pm 0.0003	0.4697 \pm 0.0003	0.4716 \pm 0.0003

TABLE II. Study of total cross section $\sigma(v_{\max})$ and charge asymmetry $A_{\text{FB}}(v_{\max})$, $d\bar{d} \rightarrow \mu^- \mu^+$, at $\sqrt{s}=189\text{GeV}$. See Table I for definition of the energy cut v_{\max} , scattering angle and M.E. type,

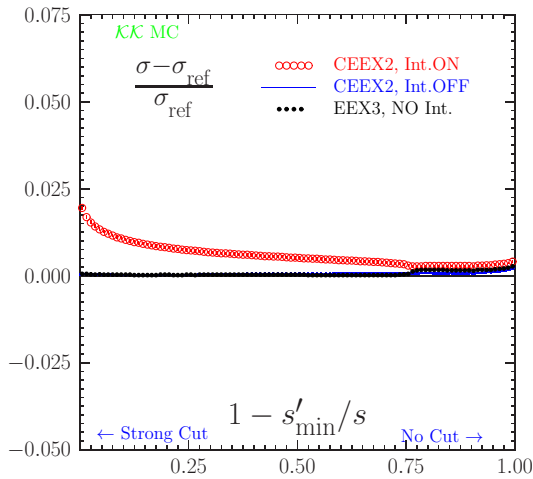


FIG. 5. Energy cut-off study of Total cross section for $d\bar{d} \rightarrow \mu^- \mu^+$, at 189GeV. The same as in the table II. σ_{ref} = semianalytical of $\mathcal{K}\mathcal{K}\text{sem}$.

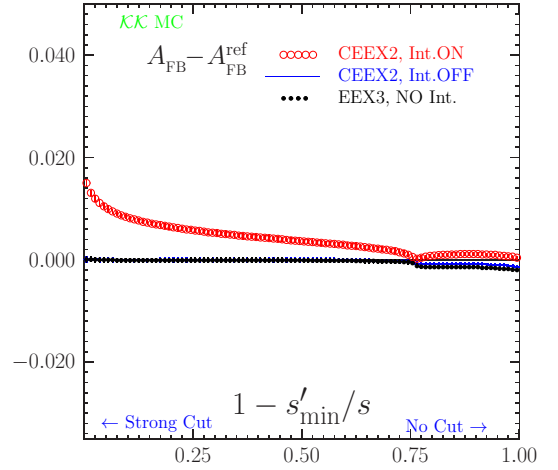


FIG. 6. Energy cut-off study of charge asymmetry A_{FB} for the process $d\bar{d} \rightarrow \mu^- \mu^+$, at 189GeV. Reference $A_{\text{FB}}^{\text{ref}}$ from semianalytical $\mathcal{K}\mathcal{K}\text{sem}$.

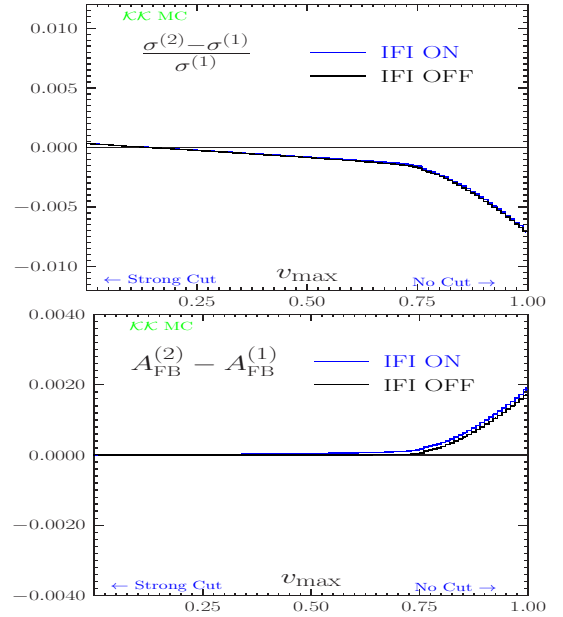


FIG. 7. Physical precision of CEEX ISR matrix element for $d\bar{d} \rightarrow \mu^- \mu^+$ at $\sqrt{s}=189\text{GeV}$. See table I for definition of cut-offs.

Turning next to the incoming $u\bar{u}$ case, we show in Tab. III and Figs. 8-10 the analogous results to those in Tab. II and Figs. 5-7 for the $u\bar{u} \rightarrow \mu^- \mu^+$ at $\sqrt{s} = 189\text{GeV}$, so that again we have the reference to the usual incoming e^+e^- annihilation case regarding the size and nature of the EW effects expected. We see that the effects are now quantitatively different, because the sizes of the EW charges are different, but they also have the opposite sign in the enhanced regions because the EW charges of the u quarks have the opposite sign to those of the e^- . This means that in the LHC environment in processes such as single Z boson production there will be some compensation between the effects from u and d quarks. A detailed application of the new $\mathcal{K}\mathcal{K}\text{MC}$ two such scenarios will ap-

pear elsewhere. Here, we specifically note that for the strong cut case with $v_{\max} = 0.01$ the IFI effect on the cross section in Tab. III is -4.14% while the effect on A_{FB} at this value of v_{\max} is -3.52% , both of which correlate well with the value of the u-quark EW charges compared to the e^- EW charges, where the corresponding results are from Tab. I 5.9% and 8.12% respectively. In Figs. 8 and 9 we show for the incoming $u\bar{u}$ the analogous plots to those in Figs. 5 and 6 for the incoming $d\bar{d}$ case of the relative values of the data in Tab. III. We see that the structure at the Z-radiative return position is a bit more evident than for the latter case and that the IFI(Initial-Final state Interference) effects are correspondingly more evident in general, as expected. In Fig. 10, we show the corresponding physical precision study as the difference between the second and first order CEEX predictions. In the worst case scenario with $v_{\max} \rightarrow 1$ we have the estimate at 0.5% on the cross section; at strong cuts $v_{\max} \rightarrow 0$ we have 0.025% and at moderate cuts near $v_{\max} \cong 0.6$ we have $.08\%$, as needed for precision LHC studies. These estimates hold for both the IFI on and IFI off cases.

v_{\max}	$\mathcal{K}\mathcal{K}\text{sem Ref.}$	$\mathcal{O}(\alpha^3)_{\text{EEX3}}$	$\mathcal{O}(\alpha^2)_{\text{CEEX intOFF}}$	$\mathcal{O}(\alpha^2)_{\text{CEEX}}$
$\sigma(v_{\max}) [\text{pb}]$				
0.01	1.2714 ± 0.0000	1.2718 ± 0.0009	1.2718 ± 0.0009	1.2191 ± 0.0009
0.10	1.6178 ± 0.0000	1.6175 ± 0.0010	1.6175 ± 0.0010	1.5792 ± 0.0010
0.30	1.8058 ± 0.0000	1.8053 ± 0.0010	1.8054 ± 0.0010	1.7784 ± 0.0010
0.50	1.9026 ± 0.0000	1.9018 ± 0.0010	1.9021 ± 0.0010	1.8815 ± 0.0011
0.70	2.0099 ± 0.0000	2.0084 ± 0.0010	2.0094 ± 0.0010	1.9938 ± 0.0011
0.90	3.3101 ± 0.0000	3.3023 ± 0.0010	3.3120 ± 0.0010	3.2993 ± 0.0010
0.99	3.3961 ± 0.0000	3.3881 ± 0.0010	3.3995 ± 0.0010	3.3872 ± 0.0010
$A_{FB}(v_{\max})$				
0.01	0.6788 ± 0.0000	0.6787 ± 0.0009	0.6787 ± 0.0009	0.6548 ± 0.0009
0.10	0.6791 ± 0.0000	0.6790 ± 0.0008	0.6790 ± 0.0008	0.6656 ± 0.0008
0.30	0.6799 ± 0.0000	0.6798 ± 0.0007	0.6798 ± 0.0007	0.6713 ± 0.0007
0.50	0.6809 ± 0.0000	0.6806 ± 0.0007	0.6806 ± 0.0007	0.6743 ± 0.0007
0.70	0.6800 ± 0.0000	0.6794 ± 0.0006	0.6793 ± 0.0006	0.6749 ± 0.0007
0.90	0.4417 ± 0.0000	0.4415 ± 0.0004	0.4407 ± 0.0004	0.4366 ± 0.0004
0.99	0.4285 ± 0.0000	0.4283 ± 0.0004	0.4274 ± 0.0004	0.4238 ± 0.0004

TABLE III. Study of total cross section $\sigma(v_{\max})$ and charge asymmetry $A_{FB}(v_{\max})$, $u\bar{u} \rightarrow \mu^-\mu^+$, at $\sqrt{s}=189\text{GeV}$. See Table I for definition of the energy cut v_{\max} , scattering angle and M.E. type,

As most of the cross section at the LHC in the single Z/γ^* production and decay to lepton pairs is concentrated near the Z-resonance, we next turn to the similar studies as we have shown in Tabs. I-III and Figs. 2-10 for $\sqrt{s} = M_Z$ so see more directly what type of effects one has to consider in precision studies of these processes. We stress that with 25fb^{-1} of recorded data for each of ATLAS and CMS, the number of such decays exceeds 10 M in each experiment. Turning first to the $d\bar{d}$ incoming beam scenario we have the results in Tab. IV and Figs. 11-13. We see that the small width(that is to say the lifetime) of the Z suppresses the IFI effects as expected: on the cross section even for the strong cut $v_{\max} = 0.01$ the effect is at the level of only 0.065% and it is already essentially non-existent at $v_{\max} = 0.1$; on A_{FB} a 5.5% enhancement at $v_{\max} = 0.01$ is already reduced to 0.29% at $v_{\max} = 0.1$. But, the effect of the radiation on the cross section is quite pronounced, as the cross section changes by 26% between the strong cut $v_{\max} = 0.01$ and the loose cut $v_{\max} = 0.99$. Thus,

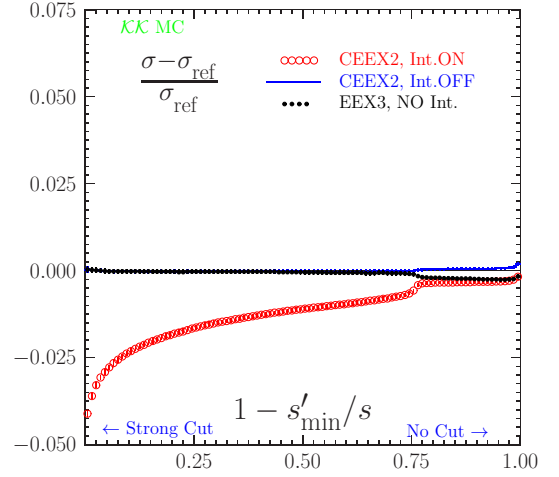


FIG. 8. Total cross section σ , energy cut-off study for the process $u\bar{u} \rightarrow \mu^+\mu^-$. The same as in the table III. No cut in θ^* . Ref. $\sigma_{\text{ref}} = \mathcal{K}\mathcal{K}\text{sem}$.

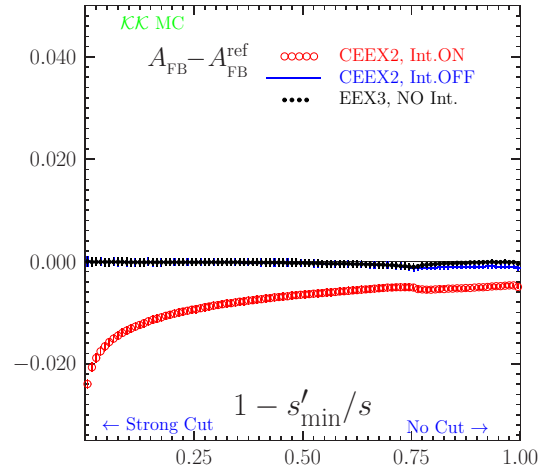


FIG. 9. Charge asymmetry A_{FB} , energy cut-off study for the process $u\bar{u} \rightarrow \mu^+\mu^-$. The same as in the table III. No cut in θ^* .

high precision on its theoretical prediction is essential for LHC precision studies. Indeed, these remarks are borne out in the plots in Figs. 11 and 12, where we respectively see the closeness of the CEEX cross section with the IFI on and IFI off and the similar closeness of the CEEX forward-backward asymmetries with the IFI on and off except for the region below $v_{\max} = 0.01$, where the IFI effect reaches 5.5% . Turning to the physical precision study in Fig. 13, we see that in the typical scenario where $v_{\max} \cong 0.6$, the precision tag for both IFI on and the IFI off cross sections is 0.04% , sufficient for the precision LHC studies.

Continuing in this vein, we present next the incoming $u\bar{u}$ scenario at $\sqrt{s} = M_Z$ in Tab. V and Figs. 14-16. We see again that the small width of the Z suppresses the IFI effects: the negative effects at $v_{\max} = 0.01$ of -0.0587% on the cross section and -16.2% on A_{FB} become respectively non-existent and -0.989% at $v_{\max} = 0.1$; at the loose cut $v_{\max} = 0.99$ the IFI effect on the cross section(the forward-backward asymmetry)

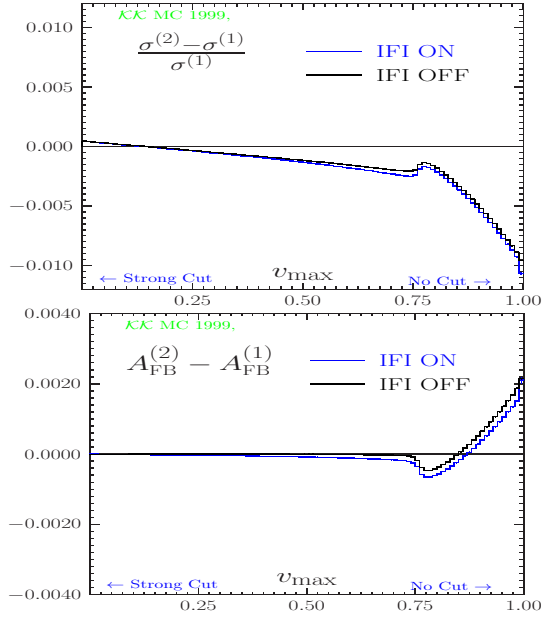


FIG. 10. Physical precision of CEE X ISR matrix element for $u\bar{u} \rightarrow \mu^- \mu^+$ at $\sqrt{s}=189\text{GeV}$. See table I for definition of cut-offs.

v_{\max}	$\mathcal{K}\mathcal{K}\text{sem Ref.}$	$\mathcal{O}(\alpha^3)_{\text{EEX3}}$	$\mathcal{O}(\alpha^2)_{\text{CEE X intOFF}}$	$\mathcal{O}(\alpha^2)_{\text{CEE X}}$
	$\sigma(v_{\max})$ [pb]			
0.01	2265.5701 ± 0.0000	2265.7449 ± 0.1721	2265.7796 ± 0.1721	2267.2517 ± 0.1796
0.10	2602.0228 ± 0.0000	2602.4244 ± 0.1519	2602.3968 ± 0.1520	2602.3923 ± 0.1620
0.30	2745.7157 ± 0.0000	2745.9432 ± 0.1385	2746.0304 ± 0.1387	2745.9989 ± 0.1500
0.50	2801.7613 ± 0.0000	2801.7212 ± 0.1317	2802.1262 ± 0.1324	2802.0849 ± 0.1443
0.70	2832.7832 ± 0.0000	2832.3374 ± 0.1275	2833.2354 ± 0.1286	2833.1826 ± 0.1409
0.90	2852.5000 ± 0.0000	2851.5051 ± 0.1246	2853.0535 ± 0.1262	2852.9951 ± 0.1388
0.99	2858.8368 ± 0.0000	2857.5479 ± 0.1237	2859.4417 ± 0.1254	2859.3787 ± 0.1381
	$A_{\text{FB}}(v_{\max})$			
0.01	0.1034 ± 0.0000	0.1033 ± 0.0001	0.1033 ± 0.0001	0.1090 ± 0.0001
0.10	0.1032 ± 0.0000	0.1031 ± 0.0001	0.1031 ± 0.0001	0.1034 ± 0.0001
0.30	0.1031 ± 0.0000	0.1031 ± 0.0001	0.1031 ± 0.0001	0.1031 ± 0.0001
0.50	0.1031 ± 0.0000	0.1031 ± 0.0001	0.1031 ± 0.0001	0.1031 ± 0.0001
0.70	0.1031 ± 0.0000	0.1031 ± 0.0001	0.1031 ± 0.0001	0.1031 ± 0.0001
0.90	0.1031 ± 0.0000	0.1030 ± 0.0001	0.1031 ± 0.0001	0.1030 ± 0.0001
0.99	0.1031 ± 0.0000	0.1030 ± 0.0001	0.1030 ± 0.0001	0.1030 ± 0.0001

TABLE IV. Study of total cross section $\sigma(v_{\max})$ and charge asymmetry $A_{\text{FB}}(v_{\max})$, $d\bar{d} \rightarrow \mu^- \mu^+$, at $\sqrt{s} = 91.187\text{GeV}$. See Table I for definition of the energy cut v_{\max} , scattering angle and M.E. type,

is below the 0.01%(0.00285) precision of the data. The cross section varies by 30.6% as v_{\max} varies from 0.01 to 0.99 so again its theoretical prediction for the radiative effects must have high precision for precision studies. These remarks are borne out by the plots in Figs. 14 and 15, where see that the IFI on and IFI CEE X cross sections are very close to the reference cross section even for the very strong and loose cuts and that the IFI on and off CEE X forward-backward asymmetries are the same as the EEX3 value by an energy cut value of 0.25, for example. In Fig. 16, we see the precision study shows that the cross section has the precision estimate of 0.04% at the energy cut of 0.6 just as we had for the incoming $d\bar{d}$ case. Again, this is sufficient for precision studies of LHC physics.

While we have discussed the individual incoming $q\bar{q}$ sce-

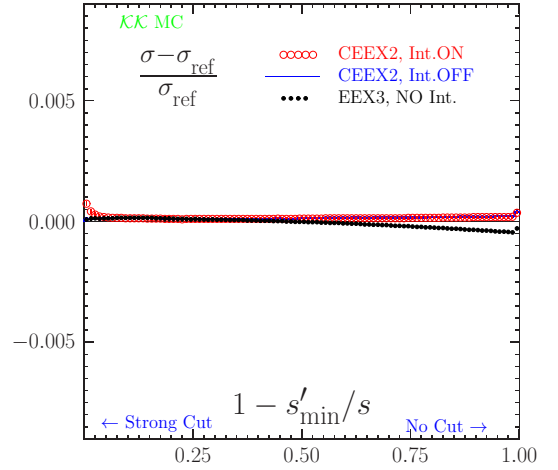


FIG. 11. Total cross section σ , energy cut-off study for the process $d\bar{d} \rightarrow \mu^- \mu^+$ at the Z. Results the same as in the table IV.

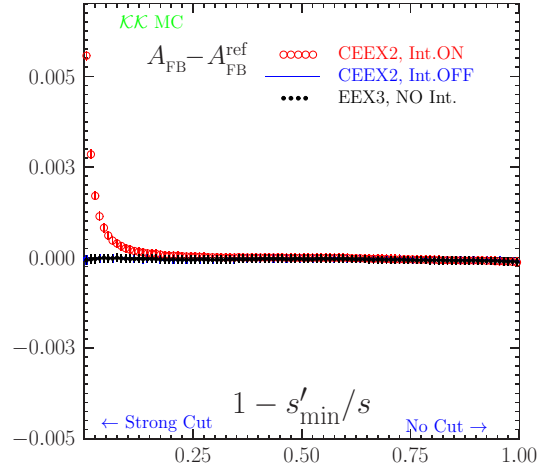


FIG. 12. Charge asymmetry A_{FB} , energy cut-off study for the process $d\bar{d} \rightarrow \mu^- \mu^+$ at the Z. Results the same as in the table IV.

narios, $\mathcal{K}\mathcal{K}\text{MC}$ 4.22 has a beamstrahlung option in which one may replace the beamstrahlung functions with the proton PDF's. We have done this as a proof of principle exercise and we show in Appendix 1 the results of a simple test run at 7TeV. What we see in this test run output is that indeed significant probability exists for the incoming quarks to radiate non-zero p_T in the higher order corrections: these effects cannot be properly described by zero p_T methods such as structure function techniques [4]. We will return to such studies elsewhere [21].

Finally, given the interest in muon collider precision physics [17], we consider next the process $\mu^+ \mu^- \rightarrow e^+ e^-$ again at $\sqrt{s} = 189\text{GeV}$, so that again we have the reference to the usual incoming $e^+ e^-$ annihilation case regarding the size and nature of the EW effects expected. In this case we have all the same EW charges but the ISR probability to radiate factor $\gamma_e = \frac{2\alpha}{\pi} (\ln(s/m_e^2) - 1) \cong 0.114$ becomes $\gamma_\mu = \frac{2\alpha}{\pi} (\ln(s/m_\mu^2) - 1) \cong 0.0649$. This means that we expect the EW effects where the photonic corrections dominate to

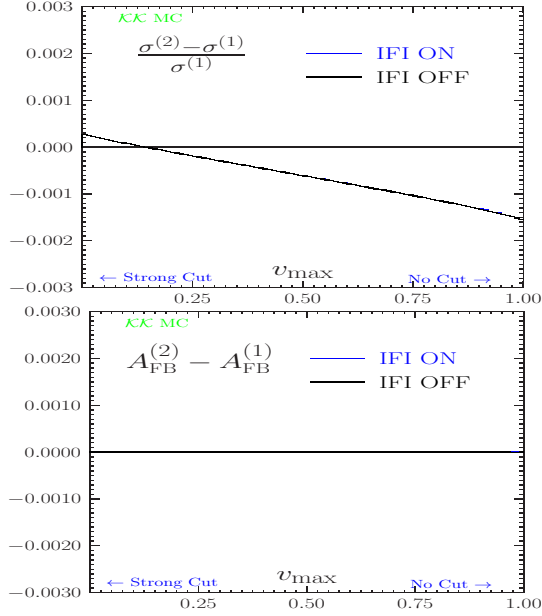


FIG. 13. Physical precision of CEEX ISR matrix element for $d\bar{d} \rightarrow \mu^-\mu^+$ at $\sqrt{s} = 91.187\text{GeV}$. See table I for definition of cut-offs.

v_{\max}	$\mathcal{K}\mathcal{K}\text{sem Ref.}$	$\mathcal{O}(\alpha^3)_{\text{EEX3}}$	$\mathcal{O}(\alpha^2)_{\text{CEEX intOFF}}$	$\mathcal{O}(\alpha^2)_{\text{CEEX}}$
$\sigma(v_{\max})$ [pb]				
0.01	1564.0869 ± 0.0000	1564.5424 ± 0.2794	1564.5808 ± 0.2794	1563.6629 ± 0.3001
0.10	1854.9598 ± 0.0000	1855.4516 ± 0.2453	1855.4499 ± 0.2453	1855.4759 ± 0.2771
0.30	1959.9902 ± 0.0000	1960.2774 ± 0.2250	1960.3844 ± 0.2252	1960.3109 ± 0.2610
0.50	2000.3461 ± 0.0000	2000.4857 ± 0.2150	2000.8275 ± 0.2155	2000.7314 ± 0.2530
0.70	2022.6577 ± 0.0000	2022.5082 ± 0.2087	2023.2161 ± 0.2095	2023.1098 ± 0.2482
0.90	2036.8954 ± 0.0000	2036.3586 ± 0.2044	2037.5580 ± 0.2055	2037.4527 ± 0.2449
0.99	2041.6520 ± 0.0000	2040.9151 ± 0.2030	2042.3715 ± 0.2042	2042.2608 ± 0.2439
$A_{\text{FB}}(v_{\max})$				
0.01	0.0736 ± 0.0000	0.0732 ± 0.0003	0.0732 ± 0.0003	0.0613 ± 0.0003
0.10	0.0712 ± 0.0000	0.0708 ± 0.0002	0.0708 ± 0.0002	0.0701 ± 0.0003
0.30	0.0708 ± 0.0000	0.0703 ± 0.0002	0.0703 ± 0.0002	0.0701 ± 0.0002
0.50	0.0707 ± 0.0000	0.0702 ± 0.0002	0.0702 ± 0.0002	0.0701 ± 0.0002
0.70	0.0706 ± 0.0000	0.0702 ± 0.0002	0.0702 ± 0.0002	0.0702 ± 0.0002
0.90	0.0706 ± 0.0000	0.0702 ± 0.0002	0.0702 ± 0.0002	0.0702 ± 0.0002
0.99	0.0706 ± 0.0000	0.0701 ± 0.0002	0.0701 ± 0.0002	0.0701 ± 0.0002

TABLE V. Study of total cross section $\sigma(v_{\max})$ and charge asymmetry $A_{\text{FB}}(v_{\max})$, $u\bar{u} \rightarrow \mu^-\mu^+$, at $\sqrt{s} = 91.187\text{GeV}$. See Table I for definition of the energy cut v_{\max} , scattering angle and M.E. type,

show reduction in size for ISR dominated regimes, the same size for the IFI dominated regimes. This is borne-out by the results in Tab. VI and Figs. 17-19. In the regime of the strong cut, with $v_{\max} = 0.01$, the results are very similar in all aspects to the usual incoming e^-e^+ case: the cross section is enhanced by 6.0% to be compared with 5.9% and A_{FB} is enhanced by 8.3% to be compared to 8.1%. In the regime of the loose cut, with $v_{\max} = 0.99$, the cross section is enhanced by 0.49% to be compared with 0.38% and A_{FB} is enhanced by 1.7% to be compared to 2.4%. In Figs. 17 and 18 we see that we have same general behavior as we have in Figs. 2 and 3, the characteristic Z peak radiative return structure in Fig. 17 and its inflection behavior in Fig. 18. In Fig. 19, we see that the precision studies comparing the second order and first order

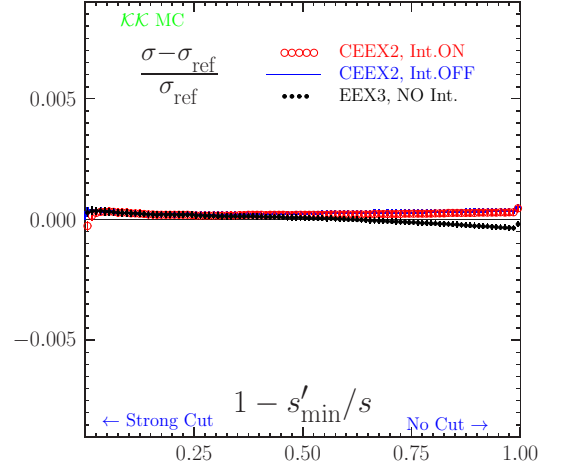


FIG. 14. Total cross section σ , energy cut-off study for the process $u\bar{u} \rightarrow \mu^+\mu^-$ at the Z peak. Results the same as in the table V.

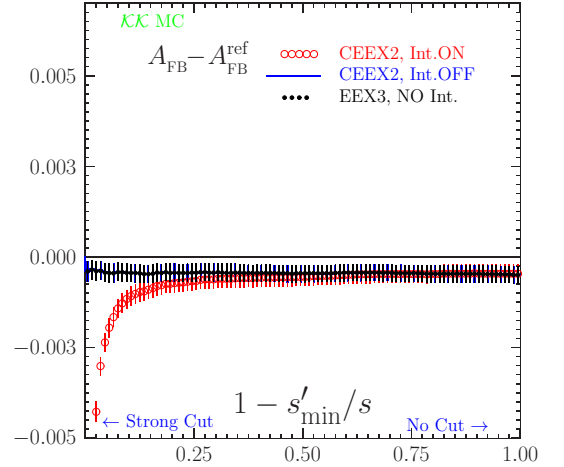


FIG. 15. Charge asymmetry A_{FB} , energy cut-off study for the process $u\bar{u} \rightarrow \mu^-\mu^+$ at the Z. Results the same as in the table V.

CEEX results show the pronounced effect of the Z radiative return. At an energy cut of 0.6, we see again that a precision tag of 0.2% obtains, so that precision results for EW effects would be available. The detailed application of such results to muon collider physics will be taken up elsewhere [28].

IV. CONCLUSIONS

YFS inspired EEX and CEEX MC schemes are successful examples of Monte Carlos based directly on the factorization theorem (albeit for the IR soft case for Abelian QED only). These schemes work well in practice: KORALZ, BHLUMI, YWSWW3, BHWIDE and $\mathcal{K}\mathcal{K}\text{MC}$ are examples. The extension of such schemes (as far as possible) to all collinear singularities would be very desirable and practically important! Work on this is in progress— see Refs. [29–31] for recent results and outlooks.

Here, we have illustrated that the $\mathcal{K}\mathcal{K}\text{MC}$ program is

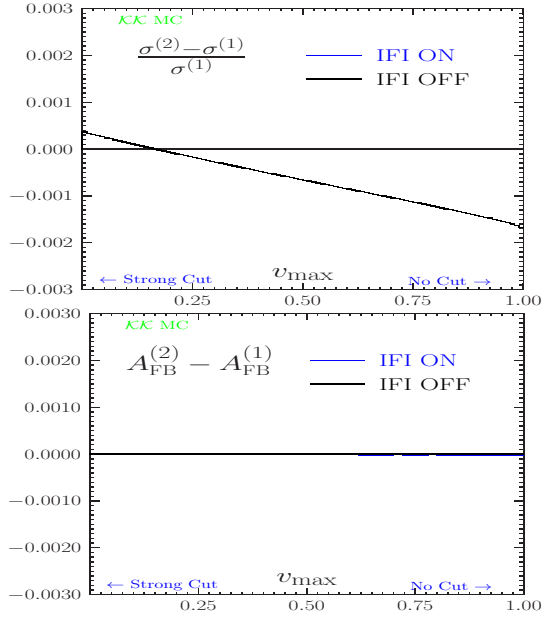


FIG. 16. Physical precision of CEEX ISR matrix element for $u\bar{u} \rightarrow \mu^-\mu^+$ at $\sqrt{s} = 91.187\text{GeV}$ (Z peak). See table I for definition of cut-offs.

v_{\max}	$\mathcal{K}\mathcal{K}\text{sem Ref.}$	$\mathcal{O}(\alpha^3)\text{EEX3}$	$\mathcal{O}(\alpha^2)\text{CEEX intOFF}$	$\mathcal{O}(\alpha^2)\text{CEEX}$
$\sigma(v_{\max})$ [pb]				
0.01	1.6703 ± 0.0000	1.6716 ± 0.0040	1.6718 ± 0.0040	1.7721 ± 0.0048
0.10	2.5076 ± 0.0000	2.5119 ± 0.0046	2.5123 ± 0.0046	2.5946 ± 0.0055
0.30	3.0153 ± 0.0000	3.0192 ± 0.0048	3.0203 ± 0.0048	3.0813 ± 0.0057
0.50	3.2808 ± 0.0000	3.2839 ± 0.0049	3.2867 ± 0.0049	3.3348 ± 0.0058
0.70	3.5252 ± 0.0000	3.5277 ± 0.0049	3.5338 ± 0.0049	3.5712 ± 0.0059
0.90	5.4288 ± 0.0000	5.3946 ± 0.0047	5.4412 ± 0.0047	5.4699 ± 0.0057
0.99	5.7248 ± 0.0000	5.6824 ± 0.0046	5.7414 ± 0.0046	5.7697 ± 0.0057
$A_{\text{FB}}(v_{\max})$				
0.01	0.5654 ± 0.0000	0.5664 ± 0.0028	0.5664 ± 0.0028	0.6132 ± 0.0032
0.10	0.5659 ± 0.0000	0.5666 ± 0.0021	0.5666 ± 0.0021	0.5934 ± 0.0025
0.30	0.5675 ± 0.0000	0.5684 ± 0.0019	0.5684 ± 0.0019	0.5855 ± 0.0022
0.50	0.5705 ± 0.0000	0.5710 ± 0.0018	0.5710 ± 0.0018	0.5835 ± 0.0021
0.70	0.5774 ± 0.0000	0.5776 ± 0.0017	0.5777 ± 0.0017	0.5870 ± 0.0020
0.90	0.3844 ± 0.0000	0.3873 ± 0.0011	0.3848 ± 0.0011	0.3921 ± 0.0012
0.99	0.3613 ± 0.0000	0.3652 ± 0.0010	0.3622 ± 0.0010	0.3683 ± 0.0012

TABLE VI. Study of total cross section $\sigma(v_{\max})$ and charge asymmetry $A_{\text{FB}}(v_{\max})$, $\mu^-\mu^+ \rightarrow e^-e^+$, at $\sqrt{s} = 189\text{GeV}$. See Table I for definition of the energy cut v_{\max} , scattering angle and M.E. type,

extended to the new incoming $f\bar{f}$, $f = \mu, \tau, \nu_\ell, q$, $q = u, d, s, c, b$, $\ell = e, \mu, \tau$, beams cases. The quark-anti-quark and $\mu^-\mu^+$ incoming beam cases are respectively important for the LHC precision EW predictions at the per mille level and to the precision EW studies for the possible muon collider physics program. We have seen that in all cases, the per mille level accuracy requirements necessitate the implementation of the $\mathcal{K}\mathcal{K}\text{MC}$ class of EW higher order effects. Realizations and applications of this class of higher order EW effects is in progress and will appear elsewhere [21]. The new version of the $\mathcal{K}\mathcal{K}\text{MC}$, version 4.22, is available at <https://jadach.web.cern.ch/jadach/KKindex.html>

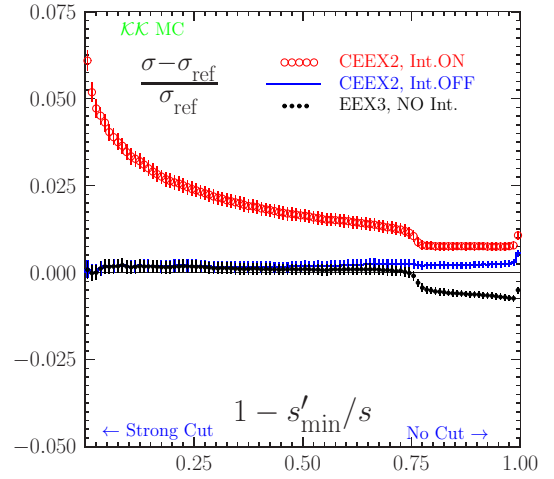


FIG. 17. Energy cut-off study of total cross section for $\mu^-\mu^+ \rightarrow e^-e^+$ at energy 189 GeV. The same results as in Table VI.

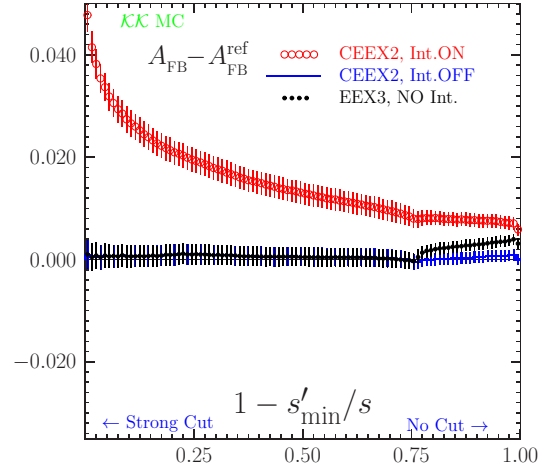


FIG. 18. Energy cut-off study of total charge asymmetry for $\mu^-\mu^+ \rightarrow e^-e^+$ at energy 189 GeV. The same results as in Table VI.

Acknowledgments

The authors thank Prof. I. Antoniadis for the support and kind hospitality of the CERN Theory Division while this work was in progress. They also thank Dr. S.A. Yost for useful discussions. One of the authors (S.J.) also thanks the Dean Lee Nordt of the Baylor College of Arts & Sciences for Baylor's support while this work was in progress. This work is partly supported by the Polish National Science Centre grant DEC-2011/03/B/ST2/02632.

Appendix A: Sample Monte Carlo events

Below sample output from run of $\mathcal{K}\mathcal{K}\text{MC}$ version 4.22 is presented for $pp \rightarrow u\bar{u} \rightarrow l^-l^+ + n\gamma$ where simple parton distribution functions (PDF's) of u and \bar{u} quarks in the proton are replacing beamstrahlung distributions (see function `BornV_RhoFoamC` in the source code). Three events are shown in the popular LUND MC format. Two photons in the event

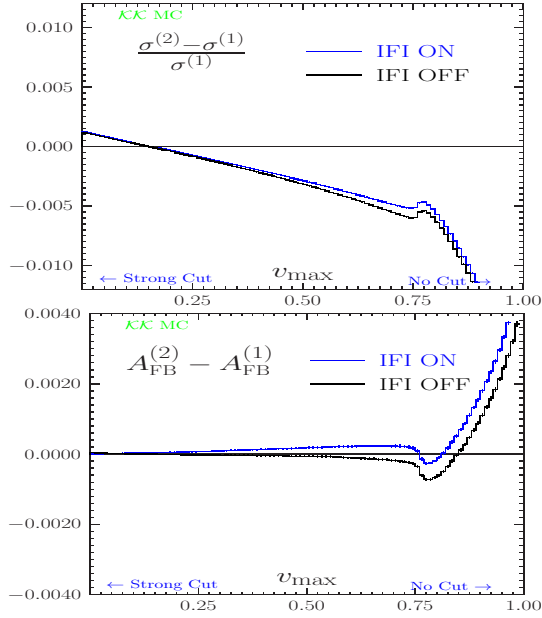


FIG. 19. Physical precision of CEEX ISR matrix element for $\mu^- \mu^+ \rightarrow e^- e^+$ at $\sqrt{s} = 189 \text{ GeV}$. See table I for definition of cut-offs.

```

*****
*                               KK Monte Carlo                               *
*                               4.22                               May 2013   *
*                               *                               *             *
*   Version                    CMS energy average                    CMSene   a1 *
*   7000.00000000              Beam energy spread                    DelEne   a2 *
*   0.00000000                 Max. photon mult.                    npmax   a3 *
*   100                         wt-ed or wt=1 evts.                  KeyWgt  a4 *
*   0                           ISR switch                            KeyISR  a4 *
*   1                           FSR switch                            KeyFSR  a5 *
*   1                           ISR/FSR interferenc                  KeyINT  a6 *
*   2                           New exponentiation                  KeyGPS  a7 *
*   1                           Hadroniz. switch                    KeyHad  a7 *
*   0                           Hadroniz. min. mass                  HadMin  a9 *
*   0.20000000                 Maximum weight                      WTmax   a10 *
*   1.00000000                 Max. photon mult.                  npmax   a11 *
*   100                         Beam ident                          KFinl   a12 *
*   0.03500000                 Manimum phot. ener.                  Ene     a13 *
*   0.10000000E-59             Phot.mass, IR regul                  MasPho  a14 *
*   1.25000000                 Phot. mult. enhanc.                  Xenph   a15 *
*   0.00000000                 PolBeam1(1)                          Pol1x   a17 *
*   0.00000000                 PolBeam1(2)                          Pol1y   a18 *
*   0.00000000                 PolBeam1(3)                          Pol1z   a19 *
*   0.00000000                 PolBeam2(1)                          Pol2x   a20 *
*   0.00000000                 PolBeam2(2)                          Pol2y   a21 *
*   0.00000000                 PolBeam2(3)                          Pol2z   a22 *
*****

Event listing (summary)
I particle/jet KS   KF orig   p_x   p_y   p_z   E   m
1 !u!           21      2      0   0.000  0.000  22.668  22.668  0.005
2 !ubar!        21     -2      0   0.000  0.000 -245.458  245.458  0.005
3 (Z0)          11     23      1  23.016  18.370 -80.068  115.249  77.487
4 gamma         1      22      1 -30.989 -6.132 -128.905  132.719  0.000
5 gamma         1      22      1  0.000  0.000  0.031  0.031  0.000
6 gamma         1      22      1  7.973 -12.238 -13.848  20.127  0.000
7 gamma         1      22      1  0.000  0.000 3477.332 3477.332  0.000
8 gamma         1      22      1  0.000  0.000-3254.542 3254.542  0.000
9 tau-          1      15      3 -24.701 21.657 -20.217  38.613  1.777
10 tau+         1     -15      3  47.716 -3.287 -59.851  76.635  1.777
sum: 0.00      0.00      0.000  0.000  0.000 7000.000 7000.000

Event listing (summary)
I particle/jet KS   KF orig   p_x   p_y   p_z   E   m
1 !u!           21      2      0   0.000  0.000  271.908  271.908  0.005
2 !ubar!        21     -2      0   0.000  0.000  -6.542  6.542  0.005
3 (Z0)          11     23      1  0.047  1.133  244.401  257.454  80.928
4 gamma         1      22      1 -0.047 -1.133  20.965  20.996  0.000
5 gamma         1      22      1  0.000  0.000 3228.092 3228.092  0.000
6 gamma         1      22      1  0.000  0.000-3493.458 3493.458  0.000
7 mu-           1      13      3  0.601  14.537  2.005  14.687  0.106
8 mu+           1     -13      3 -0.554 -13.404 242.396 242.767  0.106
sum: 0.00      0.00      0.000  0.000  0.000 7000.000 7000.000

```

record with the exactly zero transverse momentum, formerly beamstrahlung photons, are now representing proton remnants (temporary fix). What is important to see is the perfect energy momentum conservation and proper flavor structure. Overall normalization of the cross section is in principle also under strict control, however, more tests are needed.

```

Event listing (summary)
I particle/jet KS      KF orig  p_x    p_y    p_z    E      m
1 !u!          21      2      0      0.000  0.000  1816.851  1816.851  0.005
2 !ubar!       21      2      0      0.000  0.000  -1.137    1.137    0.005
3 (Z0)         11      23     1      0.011  0.003  1810.259  1812.532  90.760
4 gamma        1      22     1     -0.012 -0.002   5.371    5.371    0.000
5 gamma        1      22     1      0.000  0.000  1683.149  1683.149  0.000
6 gamma        1      22     1      0.000  0.000 -3498.863  3498.863  0.000
7 mu-          1      13     3     12.468 -25.466  1612.743  1612.992  0.106
8 mu+          1     -13     3    -12.457  25.469  197.516   199.540  0.106
sum:          0.00  -0.001  0.001  -0.084  6999.916  6999.916
*****
*                KK2f_Finalize printouts                *
* 7000.000000000 cms energy total                      cmsene a0 *
* 5000          total no of events                      nevgen a1 *
* ** principal info on x-section **                      *
* 233.95163953 +- 1.04896414 xs_tot MC R-units          xsmc a1 *
* 0.41468908      xs_tot picob.                        xSecPb a3 *
* 0.00185933      error picob.                          xErrPb a4 *
* 0.00448368      relative error                        erel a5 *
* 0.82048782      WTsups, largest WT                     WTsup a10 *
* ** some auxiliary info **                              *
* 0.00219522      xs_born picobarns                      xborn a11 *
* 0.73760000      Raw phot. multipl.                    === *
* 5.00000000      Highest phot. mult.                    === *
* End of KK2f_Finalize                                  *
*****

```

-
- [1] See for example B.F.L. Ward, *Acta Phys. Polon.* **B42**(2011) 1663, and references therein.
- [2] S. Jadach and B.F.L. Ward, *Phys. Rev.* **D38** (1988) 2897;*ibid.* **D39** (1989) 1471; *ibid.* **D40** (1989) 3582; S.Jadach, B.F.L. Ward and Z. Was, *Comput. Phys. Commun.* **66** (1991) 276; S.Jadach and B.F.L. Ward, *Phys. Lett.* **B274** (1992) 470; S. Jadach *et al.*, *Comput. Phys. Commun.* **70** (1992) 305; S.Jadach, B.F.L. Ward and Z. Was, *Comput. Phys. Commun.* **79** (1994) 503; S. Jadach *et al.*, *Phys. Lett.* **B353** (1995) 362; *ibid.* **B384** (1996) 488; *Comput. Phys. Commun.* **102** (1997) 229; S.Jadach, W. Placzek and B.F.L. Ward, *Phys. Lett.* **B390** (1997) 298; *Phys. Rev.* **D54** (1996) 5434; *Phys.Rev.* **D56** (1997) 6939; S.Jadach, M. Skrzypek and B.F.L. Ward, *Phys. Rev.* **D55** (1997) 1206; See, for example, S. Jadach *et al.*, *Phys. Lett.* **B417** (1998) 326; *Comput. Phys. Commun.* **119** (1999) 272; *Phys. Rev.* **D61** (2000) 113010; *Phys. Rev.* **D65** (2002) 093010; *Comput. Phys. Commun.* **140** (2001) 432, 475; S.Jadach, B.F.L. Ward and Z. Was, *Comput. Phys. Commun.* **124** (2000) 233; and references therein.
- [3] D. Bardin *et al.*, *JETP Lett.* **96** (2012) 285; arXiv:1207.4400; S.G. Bondarenko and A.A. Saponov, arXiv:1301.3687, and references therein.
- [4] L. Barze *et al.*, arXiv:1302.4606; C.M. Carloni-Calame *et al.*, *J. High Energy Phys.* **05** (2005) 019; G. Balossini *et al.*, *J. Phys. Conf. Ser.* **110** (2008) 042002; and references therein.
- [5] Y. Li and F. Petriello, *Phys. Rev.* **D86**(2012) 094034.
- [6] V. A. Zykunov, *Eur. Phys. J.* **C3** (2001) 9; S. Dittmaier and M. Kramer, *Phys. Rev.* **D65** (2002) 073007; S. Dittmaier and M. Huber, *J. High Energy Phys.* **1001** (2010) 060; A. Denner *et al.*, *J. High Energy Phys.* **1106** (2011) 069; and references therein.
- [7] C. Bernaciak and D. Wackeroth, *Phys. Rev.* **D85** (2012) 093003 and references therein.
- [8] LEPWWG, TEVEWWG, SLD EW and HF groups, arXiv:1012.2367, and references therein.
- [9] G. Altarelli and G. Parisi, *Nucl. Phys.* **B126** (1977) 298; Yu. L. Dokshitzer, *Sov. Phys. JETP* **46** (1977) 641; L. N. Lipatov, *Yad. Fiz.* **20** (1974) 181; V. Gribov and L. Lipatov, *Sov. J. Nucl. Phys.* **15** (1972) 675, 938; see also J.C. Collins and J. Qiu, *Phys. Rev.* **D39** (1989) 1398.
- [10] C.G. Callan, Jr., *Phys. Rev.* **D2** (1970) 1541; K. Symanzik, *Commun. Math. Phys.* **18** (1970) 227, and in *Springer Tracts in Modern Physics*, **57**, ed. G. Hoehler (Springer, Berlin, 1971) p. 222; see also S. Weinberg, *Phys. Rev.* **D8** (1973) 3497.
- [11] D. R. Yennie, S. C. Frautschi, and H. Suura, *Ann. Phys.* **13** (1961) 379; see also K. T. Mahanthappa, *Phys. Rev.* **126** (1962) 329, for a related analysis.
- [12] S. Jadach, B.F.L. Ward, Z. Wąs, *Phys. Rev. D* **63** (2001) 113009.
- [13] S. Jadach, B.F.L. Ward, Z. Wąs, *Comput. Phys. Commun.* **130** (2000) 260.
- [14] T.K.O. Doan, W. Placzek and Z. Wąs, arXiv:1303.2220; CERN-PH-TH-2013-040, IFJAN-IV-2013-2.
- [15] A.B. Arbuzov, R.R. Sadykov and Z. Wąs, arXiv:1212.6783; IFJAN-IV-2012-14, CERN-PH-TH-2012-354.
- [16] S. Jadach, B.F.L. Ward, Z. Wąs, *Eur. Phys. J.* **C22** (2001) 423; *Phys. Lett.* **B449** (1999) 97; B.F.L.Ward, S. Jadach and Z. Wąs, *Nucl.Phys.B Proc. Suppl.* **116** (2003) 116, and references therein.
- [17] See for example D.M. Kaplan, ed. (FERMILAB-CONF-12-420-APC), arXiv: 1212.4214; A. Conway and H. Wenzel, arXiv: 1304.5270; E. Eichten and A. Martin, arXiv: 1306.2609, and references therein.
- [18] F. Englert and R. Brout, *Phys. Rev. Lett.* **13** (1964) 312; P.W. Higgs, *Phys. Lett.* **12** (1964) 132; *Phys. Rev. Lett.* **13** (1964) 508; G.S. Guralnik, C.R. Hagen and T.W.B. Kibble, *ibid.* **13** (1964) 585.
- [19] F. Gianotti, in *Proc. ICHEP2012*, in press; G. Aad *et al.*, *Phys. Lett.* **B716** (2012) 1, arXiv:1207.7214.

- [20] J. Incandela, *ibid.*, 2012, in press; D. Abbaneo *et al.*, *ibid.***716** (2012) 30, arXiv:1207.7235.
- [21] S. Jadach *et al.*, to appear; V. Halyo *et al.*, to appear.
- [22] See for example K. Hamilton and P. Richardson, J. High Energy Phys. **0607** (2006) 010.
- [23] See for example M. Shonherr and F. Krauss, J. High Energy Phys. **0812** (2008) 018.
- [24] D. Bardin *et al.*, Comput. Phys. Commun. **133** (2001) 229.
- [25] F.A. Berends, W.L. Van Neerven and G.J.H. Burgers, Nucl. Phys. **B297** (1988) 429, and references therein.
- [26] S. Jadach, M. Melles, B.F.L. Ward and S. A. Yost, Phys. Rev. **D65** (2002) 073030, and references therein.
- [27] A.D. Martin *et al.*, Eur. Phys. J. **C39** (2005) 155.
- [28] S. Jadach *et al.*, to appear.
- [29] M. Slawinska, S. Jadach and K. Kutak, Phys. Lett. **B722** (2013) 151; S. Jadach *et al.*, PoS (**LL2012**) (2012) 019; Acta Phys. Polon. **B43** (2012) 2067; K. Kutak *et al.*, J. High Energy Phys. **1202** (2012) 117; and references therein.
- [30] S. Joseph *et al.*, Phys. Lett. **B685** (2010) 283; Phys. Rev. **D81** (2010) 076008; B.F.L. Ward *et al.*, Mod. Phys. Lett. **A25** (2010) 2207; B.F.L. Ward and S. Yost, PoS (**ICHEP2010**) (2011) 127; B.F.L. Ward, S.K. Majhi and S.A. Yost, PoS(**RADCOR2011**) (2012) 022; S.K. Majhi *et al.*, Phys. Lett. **B719** (2013) 367; arXiv:1305.0023; and references therein.
- [31] S. Yost *et al.*, PoS (**RADCOR2011**) (2012) 017; and references therein.